The current issue and full text archive of this journal is available at
www.emeraldinsight.com/0961-5539.htm

Thermal and fluid dynamic behaviors in symmetrical heated channel-chimney systems

Assunta Andreozzi
Dipartimento di Energetica, Termouidodinamica applicata e Condizionamenti ambientali, Università degli Studi di Napoli FEDERICO II, Napoli, Italy, and
Bernardo Buonomo and Oronzio Manca
Dipartimento di Ingegneria Aerospaziale e Meccanica, Seconda Università degli Studi di Napoli, Aversa, Italy

Received 13 January 2009
Revised 30 September 2009
Accepted 8 October 2009

Abstract

Purpose – The purpose of this paper is to evaluate the thermal and fluid dynamic behaviors of natural convection in a vertical channel-chimney system heated symmetrically at uniform heat flux in order to detect the different fluid motion structures inside the chimney, such as the cold inflow from the outlet section of the chimney and the reattachment due to the hot jet from the channel, for different extension and expansion ratios of the adiabatic extensions.

Design/methodology/approach – The model is constituted by two-dimensional steady-state fully elliptic conservation equations which are solved numerically in a composite three-part computational domain by means of the finite-volume method.

Findings – Stream function and temperature fields in the system are presented in order to detect the different fluid motion structures inside the chimney, for different extension and expansion ratios of the adiabatic extensions. The analysis allows to evaluate the effect of the channel aspect ratio on the thermal and fluid dynamic behaviors on a channel-chimney system and thermal and geometrical conditions corresponding to a complete downflow. Guidelines to estimate critical conditions related to the beginning of flow separation and complete downflow are given in terms of order of magnitude of Rayleigh and Froude numbers.

Research limitations/implications – The hypotheses on which the present analysis is based are: two-dimensional, laminar and steady-state flow, constant thermophysical properties with the Boussinesq approximation. The investigation is carried out in the following ranges: from 100 to 100,000 for the Rayleigh number, from 5.0 to 20 for the aspect ratio, from 1.0 to 4.0 for the expansion ratio and from 1.5 to 4 for the extension ratio.

Practical implications – Thermal design of heating systems in different technical fields, such as in electronic cooling and in building ventilation and houses solar components, evaluation of heat convective coefficients and guidelines to estimate critical conditions related to the beginning of flow separation and complete downflow.

Originality/value – The paper is useful to thermal designers because of its evaluation of the thermal and velocity fields, correlation for the Nusselt number and guidelines criteria in terms of Rayleigh and Froude numbers to evaluate conditions of flow separation and complete downflow in natural convection in air for vertical channels-chimney systems.

Keywords Convection, Fluid dynamics, Flow, Thermodynamics

Paper type Research paper

International Journal of Numerical Methods for Heat & Fluid Flow
Vol. 20 No. 7, 2010
pp. 811-833

0961-5539
DOI 10.1108/09615531011065584

This work is funded by the Regione Campania Legge 5 and SUN 2007 research grants.

Nomenclature

a	thermal diffusivity (m^2/s)
b	channel gap (m)
B	chimney gap (m)
Fr	Froude number, Equation (11)
g	acceleration due to the gravity $(m/s)^2$
Gr	Grashof number, Equation (5)
$h(x)$	local convective coefficient (W/m^2 K)
k	thermal conductivity (W/mK)
L	channel-chimney height (m)
L_h	channel height (m)
L_x	height of the reservoir (m)
L_y	width of the reservoir (m)
n	time step
$Nu(X)$	local Nusselt number, Equation (6)
Nu	average Nusselt number, Equation (7)
p	pressure (Pa)
P	dimensionless pressure, Equation (5)
Pr	Prandtl number, Equation (5)
$\dot{q}$	heat flux (W/m^2)
Ra	Rayleigh number, Equation (5)
Ra^*	channel Rayleigh number, Equation (5)
Re	Reynolds number, Equation (16)
T	temperature (K)
u, v	velocity components along x,y (m/s)
U, V	dimensionless velocities, Equation (5)
x, y	Cartesian coordinates (m)
X, Y	dimensionless Cartesian coordinates, Equation (5)

Greek symbols

β	volumetric coefficient of expansion (1/K)
ε	convergence criterion
η	dummy variable
θ	dimensionless temperature, Equation (5)
ν	kinematic viscosity (m^2/s)
ψ	stream function (m^2/s)
Ψ	dimensionless stream function, Equation (5)
ρ	density (kg/m^3)
ω	vorticity (1/s)
Ω	dimensionless vorticity, Equation (5)

Subscripts

∞	free stream condition
av	average value
c	cold
ch	chimney
h	hot
max	maximum value
r	reattachment
s	separation
w	wall
w_1	left wall
w_2	right wall

Introduction

Natural convection finds large employment in applications due to its simplicity, low cost and reliability, even if its heat transfer rate is low. There is the need to improve heat transfer in natural convection by means of simple geometrical modifications and to carry out geometrical parameters values for assigned configurations in order to achieve maximum heat transfer rate (Kim and Lee, 1996; Ledezma and Bejan, 1997; Bejan, 2000). The simple vertical channel has been one of the most investigated

geometry in natural convection, due to its wide engineering applications as reviewed by Gebhart *et al.* (1988), Manca *et al.* (2000) and more recently by Ayinde *et al.* (2006), Yilmaz and Gilchrist (2007) and Yilmaz and Fraser (2007).

A very simple method, which allows to improve the chimney effect and consequently heat transfer rate in vertical channels and other configurations, is to place parallel adiabatic extensions downstream of heated configurations (Haaland and Sparrow, 1983), as recently reviewed by Manca *et al.* (2000), Auletta *et al.* (2001) and Auletta and Manca (2002). However, as described by Modi and Torrance (1987), buoyant free jet at the exit zone of the ducts or parallel plates may separate from the walls before the exit section. The separation could determine a cold inflow or downflow, i.e. air from the cold ambient enters at the exit section of the system and flows downward. Later, the fluid reverses its motion following the main flow, the buoyant jet. This phenomenon can weaken the chimney effect of the system due to increased exit pressure losses. Then it is necessary to know the numerical values of geometrical, thermal and fluid dynamic parameters which give rise to cold inflow in a system with adiabatic extensions downstream.

The phenomenon of cold inflow has been investigated for some vertical geometries such as ducts (Jorg and Scorer, 1967) and channels (Modi and Torrance, 1987; Sparrow *et al.*, 1984; Moore, 1978; Modi and Moore, 1987), heat sink-chimney systems (Fisher and Torrance, 1999; Thrasher *et al.*, 2000) and channel-chimney systems (Asako *et al.*, 1990; Manca *et al.*, 2001, 2002; Oosthuizen, 1984). Jorg and Scorer (1967) carried out an experimental study to evaluate the penetration of the downflow in tubes for laminar and turbulent flow of water. They found that the presence of the inflow and its penetration depend on Reynolds number, Froude number, tube height to diameter ratio, upstream velocity profile, wall roughness and heat transfer through the wall of the tube. The inflow penetration increases with decreasing Froude number, but the effect of the other parameters was not quantified. Experiments on laminar natural convection in water, in vertical channel with one plate at uniform temperature and the other one adiabatic, was carried out by Sparrow *et al.* (1984). Flow visualization revealed downflow (flow reversals) adjacent to the upper part of the unheated walls. At low Rayleigh number (*Ra*), based on the channel gap, the cold inflow was very small but constant, whereas above a critical *Ra* the penetration length of the inflow increased linearly with *Ra*. The inflow in the upper part of the channel did not influence the heat transfer on the heated wall.

In an investigation on natural draft cooling towers, Moore (1978) observed a cold inflow under conditions of low draft velocities and large exit diameters. An analysis of cold inflow due to the separation from the wall in a vertical buoyant channel flow was attained by Modi and Moore (1987). The study was carried out for a laminar boundary layer in the range of large Reynolds numbers. The separation locations were determined as a function of Froude and Reynolds numbers. Modi and Torrance (1987) carried out an experimental and numerical study of separation of a smooth, attached buoyant flow from the wall of a duct. Experimental results were obtained for air and in the ranges of Reynolds and Froude numbers from 2,400 to 3,300 and from 0.68 to 2.69, respectively. It provided information on the onset and extent of cold inflow in turbulent regime. The numerical analysis was obtained for Reynolds numbers from 200 to 500 and Froude numbers from 1 to 5. Steady-state, two-dimensional, laminar flow solutions revealed a region of downflow near the wall of the duct which induced the separation of the wall boundary layer. The separated boundary layer merged into the buoyant jet above the duct exit. Experimental investigations on heat sink-chimney configurations, carried out in natural convection in air by Fisher and Torrance (1999) and Thrasher *et al.* (2000), confirmed, by means of flow-field measurements, the existence of cold inflow at the chimney exit. It was also observed that

the cold inflow was episodic and time-dependent. It was nearly time-periodic and occurred along the unheated side of the chimney. Experiments confirmed that a chimney, combined with free convection heat sinks, enhanced heat transfer and therefore, it allowed the use of smaller geometric dimensions to obtain the same heat dissipation. However, the periodic cold inflow at the chimney exit was found to reduce overall heat transfer. In both studies, the authors remarked that "the theory of cold inflow is incomplete" and their "results should provide a preliminary basis for further investigation."

Asako *et al.* (1990) examined numerically the heat transfer enhancement due to an unheated chimney attached to a vertical isothermal tube. They evaluated the optimum chimney diameter where the maximum amount of heat is transferred and found that, for optimum chimney diameters, the heat transfer enhancement was up to two-and-a-half times for low Rayleigh numbers and small chimney sizes. The decrease of chimney effect was determined by a cold inflow from the upper edge of the system for very large diameters of the chimney. In fact, they showed, by means of the stream function fields, that increasing the chimney diameter, a progressive decrease of dimensionless heat transfer coefficients was observed. The worsening began with the appearance of a vortex structure in the flow fields in the lower zone of the chimney and, in the worst configuration, the presence of the cold inflow up to the lowest section of the chimney was detected. Manca *et al.* (2001) carried out a comparison between channel-chimney systems with symmetrically and asymmetrically heated channels at uniform heat flux by means of local temperature measurements of the air and flow visualization. The effect of the heating mode was emphasized and it strongly affected the interaction among the hot plume rising from the channel, the cold inflow and the vortex region in the chimney corner. The flow visualization showed that, for small values of the extension ratio, a cold inflow penetrates nearly half length in an asymmetrically heated channel. It is very interesting to observe that, in simple channels with adiabatic extensions downstream, apart from channel Rayleigh number, three dimensionless geometrical parameters should also be able to affect the thermal and fluid dynamic behavior. The dimensionless geometrical parameters are: the channel aspect ratio (height of the channel/channel gap), the expansion ratio (distance between the adiabatic extensions/channel gap) and the extension ratio (total height of the channel-chimney system/height of the channel). The cold inflow was visualized also in a symmetrically heated channel with large values of the expansion ratio.

Deeper investigations for the symmetric heating were carried out by Auletta and Manca (2002) and Manca *et al.* (2002). Flow visualization gave the qualitative patterns of fluid motion in the channel and in the chimney (Manca *et al.*, 2002). At two values of the channel extension ratio ($L/L_h = 1.5$ and 4.0) and at the lower analyzed value of the expansion ratio ($B/b = 2.0$), the fluid flow expanded and reattached to the chimney walls, the flow was laminar and a stable vortex was noticed in the lower corner of the chimney. When the expansion ratio was larger, a larger spreading of the fluid occurred and the fluid did not reattach to the chimney walls, thus determining a cold air downflow. Local temperature measurements of the air flow in the channel and the chimney were carried out and presented by Auletta and Manca (2002). Different fluid motion regions were detected inside the chimney, particularly when the expansion ratio was greater than one. Different fluid motion regions were inferred from the average temperature of the air flow in the chimney and some of them were in agreement with the results of Manca *et al.* (2001, 2002). In other investigations on the channel-chimney systems (Haaland and Sparrow, 1983; Auletta *et al.*, 2001; Oosthuizen, 1984; Straatman *et al.*, 1993; Lee, 1994; Campo *et al.*, 1999), no information on cold inflow are found. A numerical simulation of natural convection in air, in a channel-chimney system, heated symmetrically at uniform heat flux was carried

out by Andreozzi *et al.* (2005). Results were given for a channel aspect ratio equal to 10 and some indication on the decrease in the chimney effect which is linked to the downflow were given. Andreozzi *et al.* (2009) carried out a parametric analysis extending the previous work (Andreozzi *et al.*, 2005) to other channel aspect ratio values. Thermal management of channel-chimney systems was accomplished in terms of maximum wall temperature, mass flow rate and average Nusselt number. Moreover, a correlation for optimal expansion ratio was also proposed.

It seems, to the best knowledge of the authors, that there are no numerical simulations on the analysis of cold inflow or downflow in a channel-chimney system.

On the basis of the remarked observations of Fisher and Torrance (1999) and Thrasher *et al.* (2000), in the present paper a detailed investigation is also given on the cold inflow in a different geometry and heating system which takes into account also the effect of the expansion ratio in the phenomenological aspect of the cold inflow inside the adiabatic chimney. The main difference with respect to Asako *et al.* (1990) is the geometry. In fact, they studied two cylindrical tubes: one heated and the other, the downstream extension, adiabatic. In the present paper is considered parallel plate channels in rectangular geometry. The main differences with respect to Modi and Torrance (1987) and Modi and Moore (1987) consist in the geometry and/or in velocity and temperature profiles at the inlet of the chimney, taking into account thermal and fluid dynamic conditions due to cold inflow from the outlet section of the chimney and hot jet from the heated channel.

In this paper a numerical simulation of natural convection in air, in a channel-chimney system, is proposed to achieve quantitative information on thermal and fluid dynamic behaviors. The geometry studied in this numerical investigation is important in different technical fields, such as in electronic cooling (Ledezma and Bejan, 1997; Auletta *et al.*, 2001; Fisher and Torrance, 1999; Thrasher *et al.*, 2000; Manca *et al.*, 2001, 2002; Oosthuizen, 1984; Straatman *et al.*, 1993; Lee, 1994; Campo *et al.*, 1999; Andreozzi *et al.*, 2005) and in building ventilation and houses solar components, as indicated by Andreozzi *et al.* (2005), Harris and Helwig (2007), Bacharoudis *et al.* (2007), Letan *et al.* (2003) and Kazansky *et al.* (2003). The results, given in terms of stream function and temperature fields, allow also to detect configurations where there is the cold inflow. This paper extends the results presented by Andreozzi *et al.* (2005) where wall temperature distributions, air velocity and temperature profiles and pressure values along the centerline of the channel were given for a channel aspect ratio equal to 10 and a Rayleigh number equal to 10^2 and 10^4. In the present paper, an in depth analysis on cold inflow or downflow in a channel chimney system taking into account geometrical, fluid dynamic and thermal behaviors in terms of dimensionless parameters such as Rayleigh, Froude and Reynolds numbers is carried out. Moreover, some criteria to evaluate the conditions corresponding to partial or complete downflow are provided. Results are presented for several values of channel aspect ratio, L_h/b, extension ratio, L/L_h, and expansion ratio, B/b, for Rayleigh numbers from 10^2 to 10^5. It is necessary to remark that the present steady-state analysis is not completely able to describe the unstable nature of cold inflow.

Problem formulation and governing equations

The investigated geometrical and physical problem is a symmetrically heated vertical channel with two downstream adiabatic extensions in order to enhance the "chimney effect." The system is depicted in Figure 1(a). In the following, the heated part is indicated as channel and the unheated part as chimney. The channel with two parallel plates is heated at uniform heat flux $\dot{q}$. The height of the plates is L_h and b is the distance between

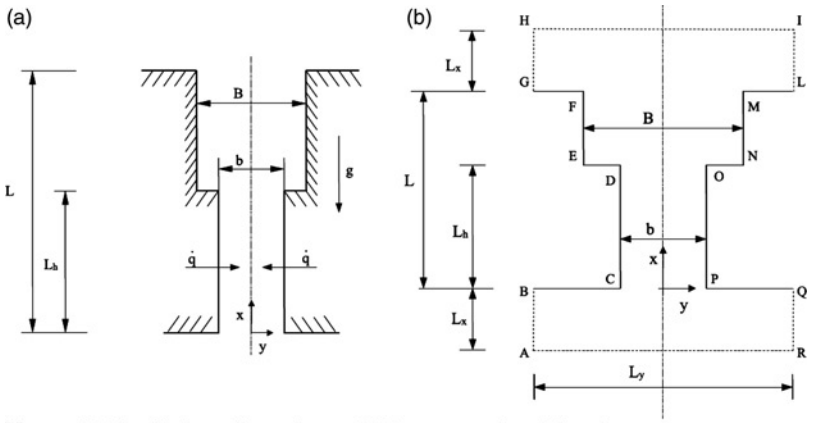

Figure 1.
Geometry of the problem

Notes: (a) Physical configuration and (b) computational domain

the two plates. Downstream the channel there is a chimney made of two adiabatic vertical parallel plates with height $(L - L_h)$ and distance between the adiabatic plates B.

The flow in the channel-chimney system is assumed to be steady-state, two-dimensional, laminar, incompressible, with negligible viscous dissipation. All thermophysical properties of the fluid are assumed to be constant, except for the dependence of the density on the temperature (Boussinesq approximation), which gives rise to buoyancy forces. With the above assumptions, the governing equations, in terms of stream-function and vorticity, which are defined as:

$$u = \frac{\partial \psi}{\partial y}; \quad v = -\frac{\partial \psi}{\partial x}; \quad \omega = \frac{\partial v}{\partial x} - \frac{\partial u}{\partial y} \tag{1}$$

are, in dimensionless form (Gebhart *et al.*, 1988):

$$\frac{\partial (U\Omega)}{\partial X} + \frac{\partial (V\Omega)}{\partial Y} = \nabla^2 \Omega - Gr \frac{\partial \theta}{\partial Y} \tag{2}$$

$$\frac{\partial^2 \Psi}{\partial X^2} + \frac{\partial^2 \Psi}{\partial Y^2} = -\Omega \tag{3}$$

$$\frac{\partial (U\theta)}{\partial X} + \frac{\partial (V\theta)}{\partial Y} = \frac{1}{Pr} \nabla^2 \theta \tag{4}$$

where the dissipative term and that involving the material derivative of the pressure were neglected, according to Gebhart *et al.* (1988).

The employed dimensionless variables are:

$$\begin{gathered} X = \frac{x}{b}, \quad Y = \frac{y}{b}, \quad U = \frac{ub}{\nu}, \quad V = \frac{vb}{\nu}, \quad P = \frac{(p - p_\infty) b^2}{\rho \nu^2} \\ \theta = \frac{(T - T_\infty) k}{\dot{q} b}, \quad \Psi = \frac{\psi}{\nu}, \quad \Omega = \frac{\omega b^2}{\nu} \\ Gr = \frac{g \beta \dot{q} b^4}{k \nu^2}, \quad Pr = \frac{\nu}{a}, \quad Ra = Gr\, Pr, \quad Ra^* = Ra(b/L_h) \end{gathered} \tag{5}$$

Following arguments raised by Straatman *et al.* (1993), Campo *et al.* (1999) and Andreozzi *et al.* (2005) an enlarged computational domain has been chosen. It is made up of the channel-chimney system and two reservoirs of height L_x and width L_y, which are placed upstream of the channel and downstream of the chimney, as illustrated in Figure 1(b) where the solid lines and the dotted lines indicate the walls and the open-boundaries, respectively. The reservoirs allow to simulate the thermal and fluid dynamic behaviors far away from the inflow and outflow regions as well as the thermal disturbance induced by the heated plates and to capture also the diffusive effects.

Equations (2-4) were solved by imposing the boundary conditions shown in Table I. They are uniform heat flux and no-slip condition on the channel plates; adiabatic wall and no-slip condition on the other solid walls; adiabatic condition for the open-boundaries of the upper reservoir and ambient temperature for the open-boundaries of the lower reservoir. Moreover, normal component of the velocity gradient equal to zero on the open-boundaries is imposed.

The local convective coefficient can be computed by means of the local Nusselt number, for the heated region as:

$$Nu(X) = \frac{h(x)b}{k} = \frac{1}{\theta_w(X)} \tag{6}$$

The average value can be written as:

$$Nu = \frac{b}{L_h}\int_0^{L_h/b} Nu(X)dX \tag{7}$$

Numerical scheme and procedure

The numerical computation was carried out with the control volume approach, using rectangular cells with constant mesh spacing. The vorticity and energy equations, Equations (2, 4), were solved by means of the alternating direction implicit method with the false transient procedure (Roache, 1998). The second-order upwind scheme (Torrance, 1985) was employed to discretize the convective derivatives, whereas the diffusive derivatives were discretized by the classical central three-point scheme.

Once the equations of vorticity, stream function and energy are solved, the following convergence criterion chosen for steady state:

Ψ	Ω	θ	Boundary
$\partial^2\Psi/\partial X^2 = 0$	$\partial\Omega/\partial X = 0$	$\theta = 0$	AR
$\partial^2\Psi/\partial Y^2 = 0$	$\partial\Omega/\partial Y = 0$	$\theta = 0$	AB and QR
$\Psi = \Psi_{w1}$	$\partial\Psi/\partial X = 0$	$\partial\theta/\partial X = 0$	BC, DE and GF
$\Psi = \Psi_{w2}$	$\partial\Psi/\partial X = 0$	$\partial\theta/\partial X = 0$	PQ, NO and LM
$\Psi = \Psi_{w1}$	$\partial\Psi/\partial Y = 0$	$\partial\theta/\partial Y = -1$	CD
$\Psi = \Psi_{w2}$	$\partial\Psi/\partial Y = 0$	$\partial\theta/\partial Y = 1$	OP
$\Psi = \Psi_{w1}$	$\partial\Psi/\partial Y = 0$	$\partial\theta/\partial Y = 0$	EF
$\Psi = \Psi_{w2}$	$\partial\Psi/\partial Y = 0$	$\partial\theta/\partial Y = 0$	MN
$\partial^2\Psi/\partial Y^2 = 0$	$\partial\Omega/\partial Y = 0$	$\partial\theta/\partial Y = 0$	GH and IL
$\partial^2\Psi/\partial X^2 = 0$	$\partial\Omega/\partial X = 0$	$\partial\theta/\partial X = 0$	HI

Table I.
Boundary conditions

$$\left| \frac{\eta_{ij}^{n+1} - \eta_{ij}^{n}}{\eta_{ij}^{n+1}} \right|_{\max} < \varepsilon \tag{8}$$

has to be checked, where η represents either Ω or θ, n the time step and ε is set equal to 10^{-6}. The computation was implemented by guessing an initial value for the stream function Ψ_{w2} at the right solid wall and assuming the stream function value equal to zero at the left solid wall, $\Psi_{w1} = 0$. The $\Delta\Psi = \Psi_{w2} - \Psi_{w1}$ represents the induced volumetric flow rate through the channel. In dimensionless terms, under the hypothesis of incompressible flow, the mass flow rate $\Delta\Psi$ is coincident with the volumetric flow rate.

Once the steady state is attained, the guessed $\Delta\Psi$ is checked by integrating the momentum equation on the centerline along the x-axis from the lower reservoir to the upper one. In fact, for the analyzed configuration, away from the entrance and exit of the channel, the pressure must be equal to that of the undisturbed environment:

$$\int_{-L_x/b}^{(L_x+L)/b} \frac{\partial P}{\partial X} dX = 0 \tag{9}$$

If the guessed value Ψ_{w2} does not satisfy this equation within a prescribed accuracy (10^{-2}), a new value of Ψ_{w2} is selected and the procedure is repeated again until the convergence of Equation (9) is obtained.

Preliminary tests were carried out to verify the accuracy of the numerical solution. Two global variables were monitored to analyze the numerical solution independence of the mesh spacing, the induced volumetric flow rate, $\Delta\Psi$, and the average Nusselt number, Nu, for a channel aspect ratio equal to 10, $L/L_h = 2.0$, $B/b = 2.0$ and $Ra = 10^4$. It was observed that by doubling the number of nodes, inside the heated channel, along Y from 11 to 21, the two global variables showed a variation of about 1.3 percent. To obtain an accurate estimate of the exact $\Delta\Psi$ and Nu values, used as reference values, a Richardson's extrapolation was used (Roache, 1998).

The variations of the induced mass flow rate and average Nusselt number values, obtained when the number of nodes along Y is 21, with respect to the reference values are 0.4 and 0.25 percent, respectively. A lesser dependence of the same variables was observed on the number of nodes along X. In the investigated cases a 71×21 uniform mesh is employed inside the heated channel for a channel aspect ratio equal to 10, whereas 35×21 and 141×21 uniform meshes are employed inside the heated channel for channel aspect ratios equal to 5 and 20, respectively.

In order to evaluated the rate of convergence of the used scheme three grids were employed as suggested by Pelletier and Roache (2006). The used grids had in the channel a number of nodes, $n_x \times n_y$, equal to 35×11, 71×21 and 141×41. The estimated order of convergence for the U and θ variables were about 1.82 and 1.64, respectively. These values confirmed a second order of convergence of the employed scheme.

An analysis has been carried out, for the configuration with $L_h/b = 10$, $L/L_h = 2.0$, $B/b = 2.0$ and $Ra = 10^4$, to set the optimal reservoirs dimensions, L_x and L_y. Three different values of L_x and L_y were considered:

(1) $L_y = 5b$ and $L_x = 0.5L$;

(2) $L_y = 11b$ and $L_x = L$; and

(3) $L_y = 15b$ and $L_x = 1.5L$.

The monitored variables are $\Delta\Psi$, Nu and the maximum velocity at exit section of the heated channel, U_{max}. The percent differences between (1) and (2) are 1.2, 1.6 and 2.1 percent for Nu, $\Delta\Psi$ and U_{max}, respectively, whereas between (2) and (3) they are 0.5, 0.8 and 1.1 percent. A reservoir horizontal dimension, L_y, equal to 11 times b and a reservoir vertical dimension, L_x, equal to the plate height L have been chosen.

A comparison between the average Nusselt numbers obtained experimentally and numerically is reported in Figure 2. The experimental values are evaluated by means of the correlation proposed by Auletta *et al.* (2001):

$$Nu = \left(\frac{L}{L_h}\right)^{0.0268} \left\{ \left[0.259 \left(Ra^* \frac{B}{b} \right)^{0.399} \right]^{-2.02} + \left[1.42 \left(Ra^* \frac{B}{b} \right)^{0.150} \right]^{-2.02} \right\}^{-1/2.02} \tag{10}$$

Discrepancies between the correlation obtained by means of experimental results and the numerical results are observed. They are due to the heat conduction inside the heated walls of the channel plates which are present in the experimental study. The discrepancies are greater for the lower average Nusselt number values. These values correspond to the lower $Ra^*(B/b)$ values where the conductive effects are greater. However, the agreement between the experimental and numerical data is acceptable.

Results and discussion

The numerical simulation has been carried out for the Rayleigh number values in the range $[10^2; 10^5]$, for a channel aspect ratio L_h/b equal to 5.0, 10 and 20 and for $Pr = 0.71$ (air). Moreover, the analyzed expansion ratios and extension ratios are in the range [1.0; 4.0] and [1.5; 4.0], respectively. Results are shown in terms of stream function and temperature fields and they also allow to detect configurations where there is the cold

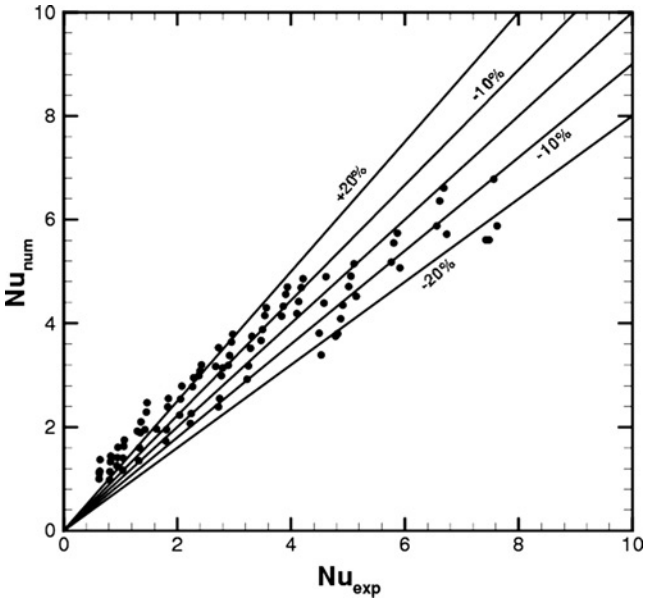

Figure 2.
Comparison between numerical (Nu_{num}), present data, and experimental (Nu_{exp}), data evaluated, equation (10), by Auletta *et al.* (2001), average Nusselt numbers

inflow. However, the present results are obtained in steady-state condition and they should take as a tentative to describe the cold inflow and they are not completely able to describe this phenomenon.

Stream function and temperature fields

Stream function and temperature fields for $L/L_h = 2.0$ and $B/b = 2{:}0$ are reported in Figures 3 and 4 for different aspect ratio values and $Ra = 10^2$ and 10^5. It should be observed that, in these figures, the X and Y scales are different to permit the fields visualization at different values of the analyzed dimensionless geometrical ratios. Stream function and temperature fields for $L/L_h = 2.0$ and $B/b = 2.0$ are reported in Figure 3 for $Ra = 10^2$ and for three channel aspect ratios, $L_h/b = 5.0$, 10 and 20. It is observed that the dimensionless mass flow rate increases as the channel aspect ratio L_h/b increases, as underlined in the stream function fields, Figures 3(a)-(c). Inside the channel, the fluid flow is parallel to the channel walls. The fluid expands inside the chimney and it stacks again to the adiabatic extensions downstream the channel outlet section. At the chimney corners E and N, in Figure 1(b), a vertical zone is present; this zone is smaller, the bigger the channel aspect ratio. The hot jet outgoing from the chimney is distinct from the entrainment of the external environment due to the fluid jet. It is observed that the hot fluid jet presents a progressive narrowing and this narrowing does not depend strongly on the channel aspect ratio L_h/b. Isotherms, Figures 3(d)-(f), show that the fluid motion inside the channel is as more thermally marked the bigger the channel aspect ratio.

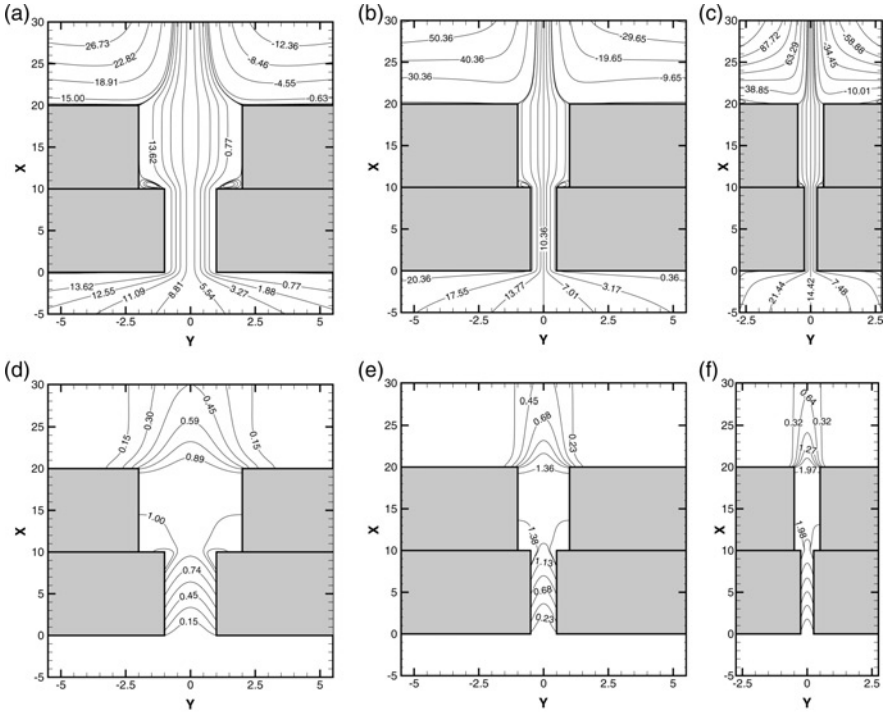

Notes: Streamlines at (a) $L_h/b = 5.0$, (b) $L_h/b = 10$, (c) $L_h/b = 20$; Isotherms at (d) $L_h/b = 5.0$, (e) $L_h/b = 10$, (f) $L_h/b = 20$

Figure 3.
Streamlines and isotherms at $Ra = 10^2$, $L/L_h = 2.0$, $B/b = 2.0$ and for different L_h/b values

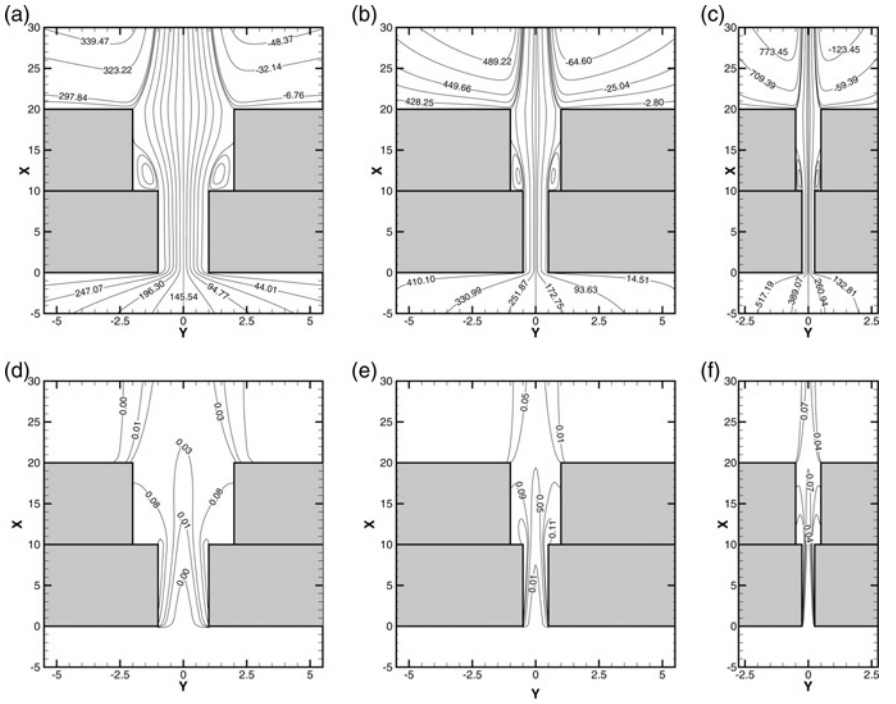

Notes: Streamlines at (a) $L_h/b = 5.0$, (b) $L_h/b = 10$, (c) $L_h/b = 20$; Isotherms at (d) $L_h/b = 5.0$, (e) $L_h/b = 10$, (f) $L_h/b = 20$

Figure 4.
Streamlines and isotherms at $Ra = 10^5$, $L/L_h = 2.0$, $B/b = 2.0$ and for different L_h/b values

Inside the chimney, it is observed that the thermal field is as less uniform as the lower L_h/b is. In fact, for $L_h/b = 5.0$, Figure 3(d), the temperature variation inside the chimney is equal to 11 percent, whereas for $L_h/b = 20$, Figure 3(f), the percentage variation is about 3.5 percent. The region in which the temperature value is the same is wider in percentage, the larger the channel aspect ratio L_h/b. For $L_h/b = 5.0$, Figure 3(d), it is clearly observed that, in the lower region of the chimney, the temperature has practically the same value as the temperature at the channel outlet section because of the presence of two vortices in the chimney corners E and N.

For the highest Rayleigh numbers here investigated, in Figure 4, it is observed that the reattachment of the fluid leaving the channel on the adiabatic walls of the chimney, downstream of the vortices, occurs at about 60 percent of the chimney height for $L_h/b = 5$:0, Figure 4(a), and at about 50 percent of the chimney height for $L_h/b = 20$, Figure 4(c).

Stream function fields for the channel aspect ratio $L_h/b = 10$ and the Rayleigh number equal to 10^2 are reported in Figure 5 for different extension ratios and for $B/b = 2.0$ and $B/b = 4.0$. In Figures 5(a)-(c), stream function field shows that the contraction of the thermal plume, outgoing from chimney, is greater for $L/L_h = 1.5$. Moreover, increasing L/L_h the mass flow rate increases and the reattachment of the fluid to the adiabatic walls inside the chimney moves slightly downstream. For $B/b = 4.0$ and $L/L_h = 1.5$, in Figure 5(d), the downflow penetrates completely inside the chimney and reaches the heated channel outflow section. The vortex zones at the two corners of the chimney disappear. For higher extension ratios, $L/L_h = 3.0$ and 4.0, in Figures 5(e) and

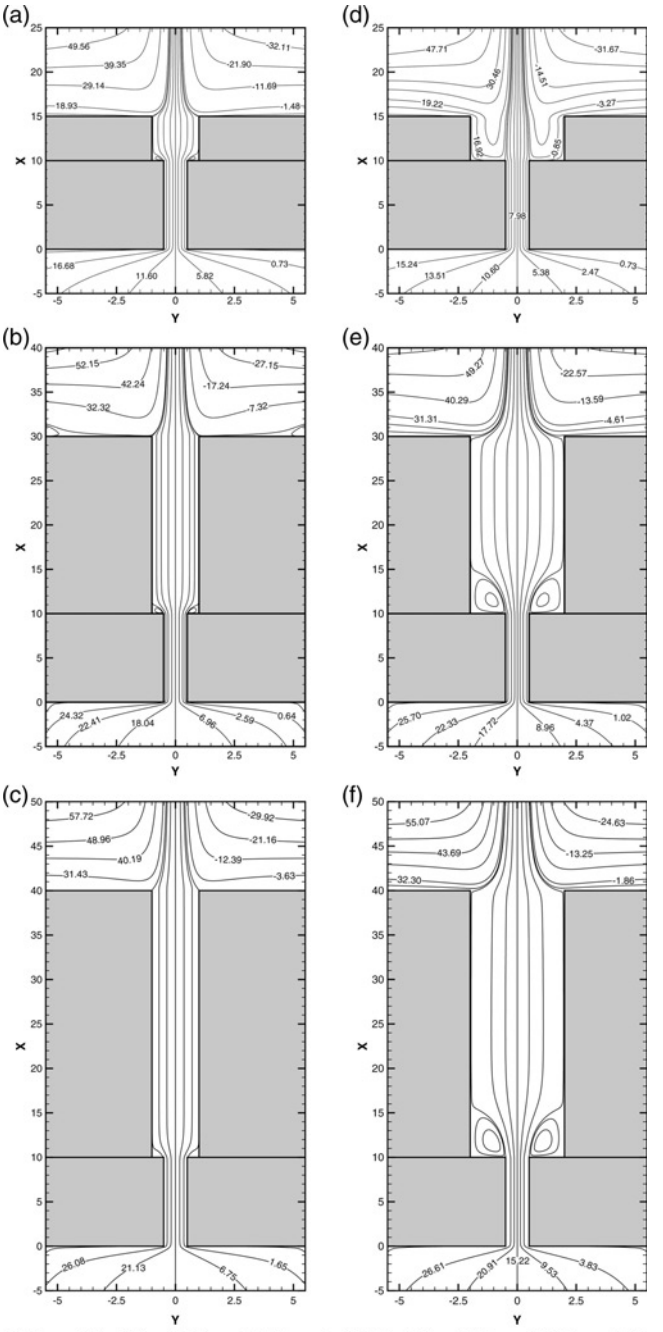

Notes: (a) $B/b = 2.0$ and $L/L_h = 1.5$; (b) $B/b = 2.0$ and $L/L_h = 3.0$; (c) $B/b = 2.0$ and $L/L_h = 4.0$; (d) $B/b = 4.0$ and $L/L_h = 1.5$; (e) $B/b = 4.0$ and $L/L_h = 3.0$ and (f) $B/b = 4.0$ and $L/L_h = 4.0$

Figure 5.
Streamlines at $Ra = 10^2$, $L_h/b = 10$ and for different L/L_h values

(f), the fluid flow presents a separation in the upper part of the adiabatic walls and a small downflow is observed. The size of the vortex cells adjacent to the corners inside the chimney increases significantly with respect to the previous cases for $B/b = 2.0$. The reattachment of the fluid flow occurs at about $X = 16$ for both cases, Figures 5(e) and (f), and about 1/4 and 1/6 of the chimney height for $L/L_h = 3.0$ and 4.0, respectively.

Stream function fields for the channel aspect ratio $L_h/b = 10$ and the Rayleigh number equal to 10^5 are reported in Figure 6 for different extension ratios and for $B/b = 2.0$ and $B/b = 4.0$. In Figure 6(a), for $L/L_h = 1.5$ and $B/b = 2.0$ it is noted that the downflow inside the chimney is complete like at the largest considered value of B/b at $Ra = 10^2$. There are two symmetrical vortex cells between the thermal plume, coming from the heated channel, and the cold inflow flowing along the adiabatic walls of the chimney. Moreover, the cold inflow, due to the downflow, is dragged out the chimney by the hot plume. The vortices extension in the corners of the chimney, for $L/L_h = 3.0$ and 4.0, in Figures 6(b) and (c), is greater than in the previous case at $Ra = 10^2$. Consequently, the fluid reattaches at about $X = 18$ and 21 for $L/L_h = 3.0$ and 4.0, respectively, at about 40 percent of the chimney height. For $B/b = 4.0$, in Figures 6(d)-(f), the downflow inside the chimney is present in all cases and a slight contraction inside the chimney of the plume incoming from the heated channel is observed. In these configurations, the downflow is due mainly to the possible extension of the vortices, adjacent to the corners of the chimney. It is greater than the height of the chimney, so that the reattachment of the fluid flow on the adiabatic walls of the chimney is not allowed.

Cold inflow and reattachment

After the aforementioned observations on the stream function and temperature fields, it is very clear that the presence of cold inflow or downflow inside the chimney determines the worsening of the system in terms of maximum wall temperature increase due to the mass flow rate decrease. As noted in the previous analysis, the cold inflow inside the chimney can be linked to two different phenomena:

(1) the separation of fluid from the outlet section of the chimney; and

(2) the position of the reattachment point on the adiabatic walls of the chimney.

As far as the authors are concerned, no previous investigations were given on the simultaneous effects of the (1) and (2) phenomena.

As already discussed in the introduction, the cold inflow, due to the separation at the outlet section, has been studied by different authors, such as Modi and Torrance (1987), Jorg and Scorer (1967), Sparrow *et al.* (1984), Moore (1978), Modi and Moore (1987), Fisher and Torrance (1999), Thrasher *et al.* (2000) and some very interesting results were given, although the theory of this phenomenon is incomplete as underlined by Fisher and Torrance (1999) and Thrasher *et al.* (2000). However, the Froude number is a fundamental dimensionless parameter in the cold inflow analysis in presence of separation from the adiabatic wall (Modi and Torrance, 1987; Modi and Moore, 1987; Fisher and Torrance, 1999). In this case, the two main and opposite forces are the inertial and buoyancy forces and at lower Froude number, the separation location moves upstream on the adiabatic wall (Modi and Torrance, 1987; Fisher and Torrance, 1999).

The Froude number is defined as by Fisher and Torrance (1999):

$$Fr = \frac{\rho_c u_{av,ch}^2}{gB(\rho_c - \rho_h)} \tag{11}$$

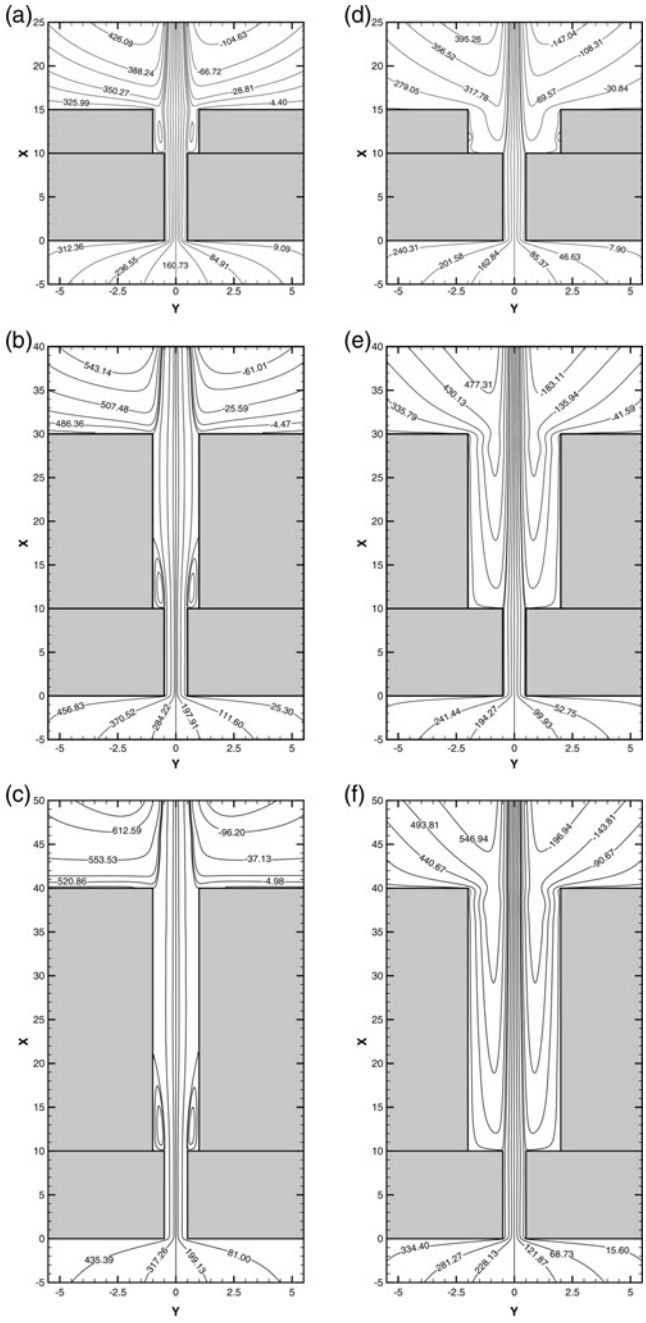

Figure 6.
Streamlines at $Ra = 10^5$, $L_h/b = 10$ and for different L/L_h values

Notes: (a) $B/b = 2.0$ and $L/L_h = 1.5$, (b) $B/b = 2.0$ and $L/L_h = 3.0$, (c) $B/b = 2.0$ and $L/L_h = 4.0$, (d) $B/b = 4.0$ and $L/L_h = 1.5$, (e) $B/b = 4.0$ and $L/L_h = 3.0$ and (f) $B/b = 4.0$ and $L/L_h = 4.0$

where $u_{av,ch}$ is the average velocity in a section of the chimney and c is cold and h is hot, i.e. the external ambient and the thermal plume incoming from the heated channel in the present study. Moreover, it is:

$$\rho_c - \rho_h \cong \rho_c \beta \Delta T \tag{12}$$

and,

$$u_{ac,ch}^2 \cong g\beta \Delta T L \tag{13}$$

Then,

$$Fr = \frac{L}{B} = \frac{(L/L_h)(L_h/b)}{B/b} \tag{14}$$

Equation (14) allows a simple analysis of the possible downflow from the outlet section of the chimney. For fixed extension and aspect ratios, the higher expansion ratio, the lower the Froude number and the higher is the possibility of the cold inflow (Modi and Torrance, 1987; Fisher and Torrance, 1999). Moreover, at higher (L/L_h) and (L_h/b), the Froude number is higher. The average velocity in the chimney is equal to $u_{av,ch} = u_{av}(b/B)$ where u_{av} is the mean velocity in the heated channel.

The Froude number is also evaluated by means of the relationship:

$$Fr = \frac{Re^2 Pr}{Ra(B/b)^3} \tag{15}$$

The Reynolds number is defined as:

$$Re = \frac{u_{av} b}{\nu} \tag{16}$$

and it is equal to the dimensionless stream function difference, which is the dimensionless volumetric flow rate. This last quantity is a function of the Rayleigh number, the expansion and extension ratios and Equation (15) can be written as:

$$Fr = \frac{\left[f\left(Ra, \frac{B}{b}, \frac{L}{L_h} \right) \right]^2 Pr}{\left(Ra \frac{B}{b} \right) \left(\frac{B}{b} \right)^2} \tag{17}$$

Successively the distance from the channel exit section, where the flow separation on the adiabatic wall of the chimney is attained, is indicated as X_s.

The reattachment of the fluid flow in the chimney for $B/b > 1.0$ could be as a phenomenon, related to the Coanda effect. The reattachment is due to the fluid expansion inside the chimney and, as observed by Kazansky *et al.* (2003), the basic mechanism of the interaction has been shown to be the restriction imposed on the fluid entrained downstream by the thermal plume, due to the presence of the neighboring surfaces or other flows. The demand for entrainment results in a pressure difference, which causes

the ambient fluid to be drawn into the plume. A neighboring surface curtails this entrainment and, thus causes a pressure imbalance which forces the thermal plume towards the surface. The resulting interaction has been found to be quite sensitive to the geometry of the flow configuration, according to Agarwal and Jaluria (1989).

In the present study, the thermal plume expands for $B/b > 1{:}0$ and the point where the reattachment on the adiabatic wall of the chimney is attained is indicated with X_r. Its value depends on the pressure difference between the plume core and the external zone and the buoyancy force. If X_r is greater than $(L - L_h)/b$, the thermal plume does not reattach to the adiabatic wall of the chimney and a complete downflow occurs inside the chimney. Moreover, if there is also a separation on the adiabatic wall, the complete downflow occurs for a value of X_r greater than X_s, but lower than $(L - L_h)/b$. The thermal plume could not attach for large B/b value and/or for large Rayleigh number. The evaluation of X_s and X_r is obtained, as suggested by Modi and Torrance (1987), by the position along the adiabatic wall of the chimney where the vorticity goes to zero.

The Reynolds number values, as a function of $Ra(B/b)$, are reported in Figure 7(a), for the three analyzed L_h/b values. It is observed that, increasing the Rayleigh number, the Reynolds number value increases and therefore increases the mass flow rate. At the same Ra value, it is noticed that the mass flow rate increases at increasing channel aspect ratio, L_h/b, at the same expansion and extension ratios. Moreover, in agreement with the streamlines fields shown in Figures 3-6 and Auletta *et al.* (2001), Asako *et al.* (1990), Straatman *et al.* (1993), Andreozzi *et al.* (2005), at increasing B/b ratio, the Reynolds number, that is the mass flow rate, reaches maximum values, due to the variation of the fluid flow inside the chimney. These variations are caused by the downflow presence which determines the decrease of the chimney effect. It is remarked that, at same L_h/b and B/b, higher Reynolds numbers correspond to higher L/L_h values. For the lower Ra values here considered, 10^2 and 10^3, the values of the expansion ratio pertinent to the maximum Reynolds number value are about 2.0 for $L/L_h \leq 2{:}0$, whereas they increase at increasing L/L_h. At increasing Rayleigh number value, 10^4 and 10^5, the B/b values pertinent to the maximum Re values remain between 1.5 and 2.0 for an assigned extension ratio. This indicates that for the higher Rayleigh number values ($\geq 10^4$), the downflow is present also for not too high B/b values (≈ 2.0).

A more immediate analysis about the configurations, in which the cold inflow and the complete downflow are present, is obtained by means of Figure 7(b), where the Froude number value, as a function of the term $Ra(B/b)$, is reported. In this figure, the configurations with separation and complete downflow are indicated; these configurations are dependent on L_h/b, too. At $B/b = 1.0$ and 1.5, for the analyzed Rayleigh number range and for all the L_h/b values, there is no separation of the flow from the adiabatic walls of the chimney. For $Ra = 10^2$ and $L_h/b = 5.0$, the separation is present for $L/L_h = 1.5$ and $B/b = 2.0$, as it can be observed in Table II, whereas the complete downflow is present for $B/b = 3.0$ and $L/L_h = 1.5$ and for $B/b = 4.0$ up to $L/L_h = 2.0$. For the other configurations the separation of the fluid from the wall is present; it increases at increasing B/b because the average velocity inside the chimney decreases and the Froude number value decreases, too. Moreover, the separation decreases at increasing extension ratio because the system draught increases and consequently the velocity inside the chimney increases, at the same B/b value. This can be observed in Table II. By increasing the channel aspect ratio, L_h/b, the fluid penetration, due to the separation, decreases because the induced mass flow rate and the average velocity increase for assigned L/L_h and B/b values. The number of configurations with a complete downflow increases at increasing Ra value whereas the

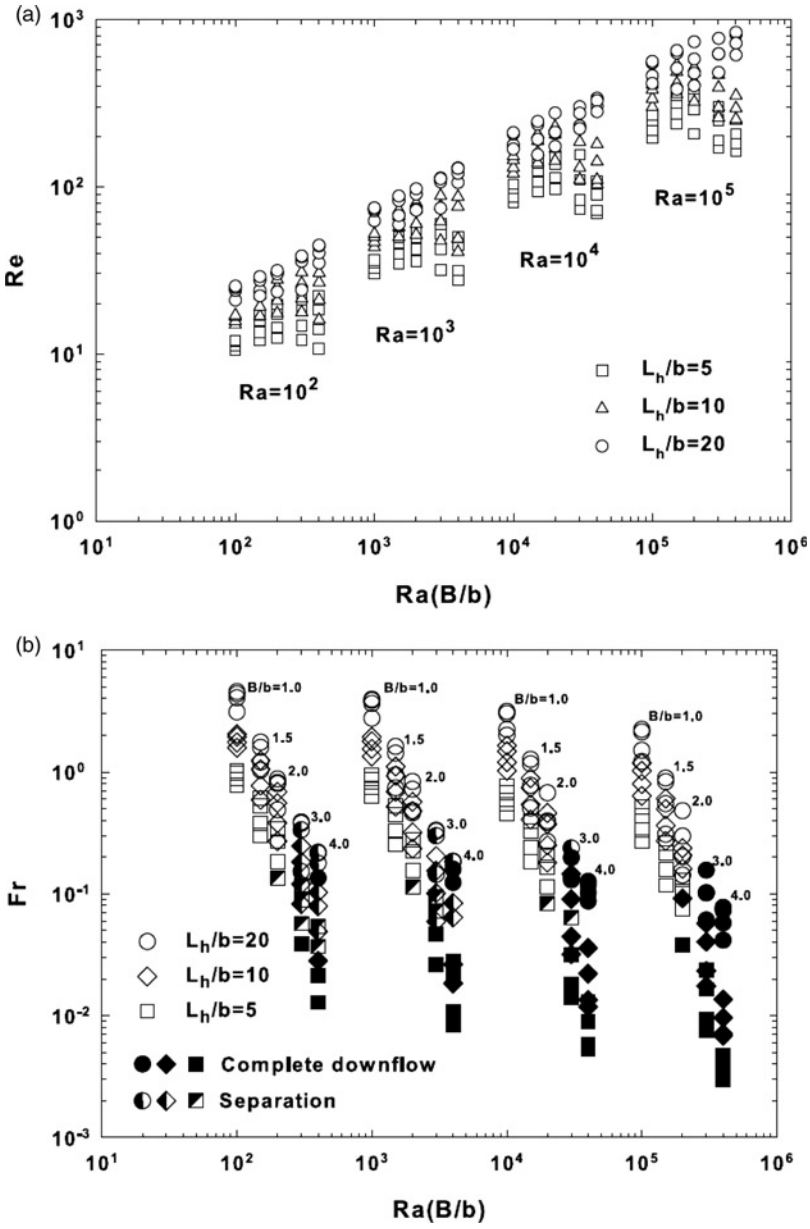

Figure 7.
Reynolds number (a) and Froude number (b) values as a function of $Ra(B/b)$ for the three analyzed L_h/b values

number of configurations with a partial separation from the wall decreases, as it is observed in Table II and in Figure 7(b). The separation is present for $B/b = 2.0$ only when L/L_h is equal to 1.5 at $Ra \leq 10^4$ whereas, for $Ra = 10^5$, only a complete downflow is observed. Furthermore, it is observed, in terms of Fr, that for $Ra = 10^2$ the separation appears for $B/b = 3.0$ and $0.3 < Fr < 0.4$, $L/L_h = 2.0$ and $L_h/b = 20$, whereas the complete downflow starts for $Fr \approx 0.15$, $L/L_h = 1.5$ and $B/b = 4.0$ with

Table II.
Xs/(*Lh*/*b*) values and full downflow (DF) at different channel aspect ratios, expansion ratios and extension ratios, in the range $10^2 \leq Ra \leq 10^5$

		$Ra = 10^2$			$Ra = 10^3$			$Ra = 10^4$			$Ra = 10^5$		
L_h/b	B/b L/L_h	2.0	3.0	4.0	2.0	3.0	4.0	2.0	3.0	4.0	2.0	3.0	4.0
5	1.5	0.498	DF	DF	0.496	DF	DF	0.492	DF	DF	DF	DF	DF
	2.0		0.984	DF		DF	DF		DF	DF		DF	DF
	3.0		1.992	1.934		1.996	DF		DF	DF		DF	DF
	4.0		2.992	2.976		2.996	DF		2.992	DF		DF	DF
10	1.5		0.479	DF		DF	DF		DF	DF	DF	DF	DF
	2.0		0.989	0.889		0.988	DF		DF	DF		DF	DF
	3.0		1.994	1.979		1.997	1.965		DF	DF		DF	DF
	4.0			2.990			2.995		2.997	DF		DF	DF
20	1.5		0.487	DF		0.474	DF		DF	DF		DF	DF
	2.0		0.992	0.956		0.995	DF		DF	DF		DF	DF
	3.0		1.999	1.987			1.989		DF	DF		DF	DF
	4.0			2.972			2.994		2.991	DF		DF	DF

$L_h/b = 20$. Figure 7(b) permits to observe that, for $Fr \leq 0{:}2$, the separation is present in almost all configurations. The minimum value of the Froude number, under which most configurations present a complete downflow, increases at increasing Rayleigh number, in agreement with Modi and Torrance (1987). In fact, this value is equal to 0.04 for $Ra = 10^2$ and it is equal to about 0.18 for $Ra = 10^5$.

In the chimney-channel system, the complete downflow can be due, not only to the separation, but also to the possibility that the hot jet, coming out the channel, does not reattach to the wall for $B/b > 1.0$. The value of X_r on the channel aspect ratio, L_h/b, as a function of $Ra(b/L_h)(B/b) = Ra^*(B/b)$ is reported in Figure 8.

In this figure, it is noted that for $B/b = 1.5$ the reattachment is always present and it is very distant from the outlet section of the chimney. As it is expected, $X_r(b/L_h)$ increases by increasing the term $Ra^*(B/b)$. Increase in the expansion ratio, the term $X_r(b/L_h)$ increases, at the same Ra^* and, in agreement with the previous results, it is noted that the number of configurations without reattachment and with a complete downflow increases. The critical

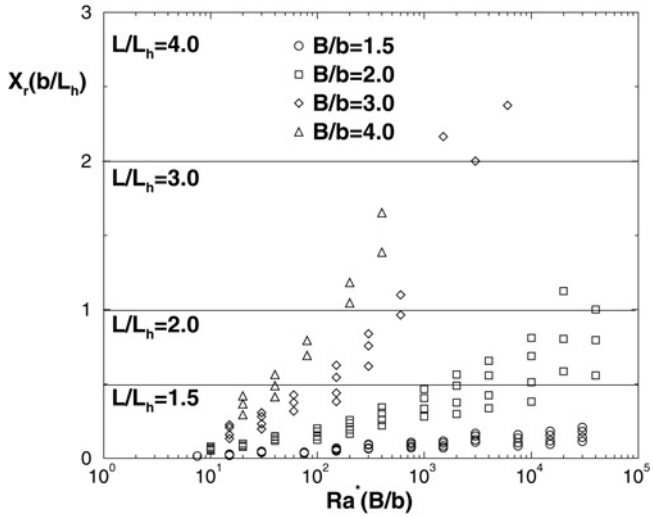

Figure 8.
X_r value on the channel aspect ratio, L_h/b, as a function of $Ra^*(B/b)$ for the different analyzed expansion and extension ratios

values of Ra for which there is no more reattachment are reported, as order of magnitude, in Table III for the different analyzed configurations. As observed, for $B/b = 1.5$ and all analyzed L_h/b values, the reattachment is always present whereas for $B/b = 2.0$ and $L/L_h = 1.5$ there is no reattachment for some configurations and so there is the complete downflow for $L_h/b = 5.0$ and 10, for $Ra > 10^4$, and $Ra = 10^4$ is the order of magnitude of the critical Ra value. For $B/b = 4.0$ and $L/L_h = 1.5$, the complete downflow is present for $Ra = 10^2$, for all L_h/b considered and the order of magnitude of the critical Ra value could be less than 10^2. The values in Table III are in very good agreement with Equation (14).

Finally a composite correlation of the average Nusselt number as a function of the channel Rayleigh number, $Ra^* = Ra(b/L_h)$, and of the expansion and extension ratios is proposed:

$$Nu = \left(\frac{B}{b}\right)^{-0.250}\left(\frac{L}{L_h}\right)^{0.150}\left\{\left[0.570\left(Ra^*\frac{B}{b}\right)^{0.306}\right]^{-11} + \left[1.155\left(Ra^*\frac{B}{b}\right)^{0.161}\right]^{-11}\right\}^{-\frac{1}{11}} \quad (18)$$

with $r^2 = 0.984$ in the ranges: $10^2 \leq Ra \leq 10^5$, $1.5 \leq L/L_h \leq 4.0$, $1.0 \leq B/b \leq 4.0$ and $5.0 \leq L_h/b \leq 20$.

In Figure 9 the data obtained numerically are compared with Equation (18) and a good agreement is observed.

Conclusions

An in-depth investigation on fluid motion behaviors, in a vertical channel-chimney system, due to natural convection was carried out numerically. The channel was heated symmetrically at uniform heat flux and results were obtained for air at steady state. The analysis of results was accomplished in terms of stream function and temperature fields in order to detect, in the chimney, the possible separation of the fluid to the adiabatic wall of the chimney, complete downflow and reattachment of the hot jet coming from the heated channel on the chimney wall for an expansion ratio, B/b, greater than 1:0, in a Rayleigh number range from 10^2 to 10^5, for different channel aspect ratios (5.0, 10 and 20) and extension ratio, L/L_h, between 1.5 to 4.0. The analysis extended the results provided by Andreozzi *et al.* (2005) allowing to obtain useful information on the effect of the channel aspect ratio, L_h/b, and on thermal and geometrical conditions corresponding to the complete downflow. The evaluation of the flow separation and reattachment along the adiabatic wall of the chimney was obtained by means of the analysis employed by Modi and Torrance (1987).

L/L_h	$L_h/b = 5.0$				$L_h/b = 10$				$L_h/b = 20$			
B/b	1.5	2.0	3.0	4.0	1.5	2.0	3.0	4.0	1.5	2.0	3.0	4.0
1.5	$>10^5$	$>10^5$	$>10^5$	$>10^5$	$>10^5$	$>10^5$	$>10^5$	$>10^5$	$>10^5$	$>10^5$	$>10^5$	$>10^5$
2.0	10^4	$>10^5$	$>10^5$	$>10^5$	10^4	$>10^5$	$>10^5$	$>10^5$	$>10^5$	$>10^5$	$>10^5$	$>10^5$
3.0	$<10^2$	10^2	10^3	10^4	10^2	10^3	10^3	10^4	10^3	10^3	10^3	10^4
4.0	$<10^2$	$<10^2$	10^2	10^2	$<10^2$	10^2	10^3	10^3	$<10^2$	10^2	10^3	10^3

Table III. Critical Rayleigh numbers for which there is no reattachment on the chimney walls

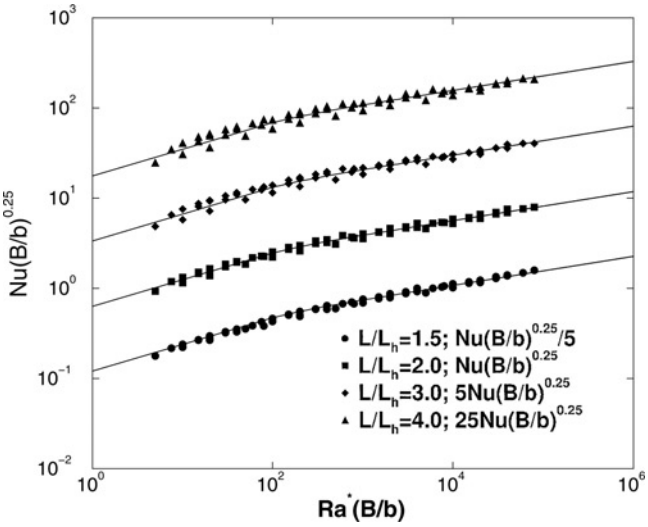

Figure 9.
Comparison between numerical data and composite correlation in Equation (17)

Results in terms of stream function and temperature fields allowed the flow visualization in the chimney in order to detect the different structures of the fluid motion for various configurations. This analysis enabled an understanding that, in the channel-chimney system, the cold inflow is linked both to the contraction of the thermal plume coming out from the chimney and the expansion of the hot jet arising from the channel for $B/b > 1{:}0$. These effects were high at greater expansion ratio and lower at higher extension ratio. Increasing the Rayleigh number, the reattachment on the chimney walls occurred at a distance further from the channel outlet section and the thermal plume contraction decreased.

It was observed, by means of the analysis of the Reynolds number, as a function of the term $Ra(B/b)$, that increasing the channel aspect ratio, the mass flow rate increased and an optimum value of the mass flow rate, with respect to B/b, in agreement with Auletta *et al.* (2001), Asako *et al.* (1990), Straatman *et al.* (1993), Andreozzi *et al.* (2005), was detected. The optimal B/b was a function of Ra, L_h/b and L/L_h and it decreased at increasing Ra and increased at increasing L/L_h.

Some possible guidelines, to evaluate critical conditions related to the beginning of flow separation and complete downflow, were provided as order of magnitude of Rayleigh and Froude numbers. In fact, it was found that, for lower Ra value, ~10^2, flow separation starts for $Fr < 0.4$ when $B/b = 3.0$. The complete downflow was observed for $B/b = 2.0$ and $L_h/b = 10$ only for $Ra = 10^5$ and $L/L_h = 1.5$. For $B/b = 3.0$, the critical Froude number, under which there is always the complete downflow, increased at increasing Ra value and it was 0.04 for $Ra = 10^2$ and about 0.18 for $Ra = 10^5$. Some indications to identify complete downflow, in terms of geometrical parameters and Ra, were evaluated.

Finally, a composite correlation for the average Nusselt number, in terms of channel Rayleigh number, extension and expansion ratios, was proposed in the Rayleigh number range from 10^2 to 10^5, for $L_h/b = 5.0$, 10 and 20, $1.0 \leq B/b \leq 4.0$ and $1.5 \leq L/L_h \leq 4.0$. The equation was in a very good agreement with numerical data.

This investigation, although obtained for steady state, is in agreement with what was suggested in the numerical analysis carried out by Modi and Torrance (1987), but

it should be remarked that a complete description of the cold inflow or downflow is not possible due to the unsteady nature of this phenomenon, as observed by Modi and Torrance (1987), Fisher and Torrance (1999) and Thrasher (2000). However, the results given in this investigation are a tentative to provide useful guidelines to determine, in terms of Rayleigh and Froude numbers, if a channel-chimney system, with assigned thermal and geometrical parameters, is in critical condition related to flow separation, complete downflow and reattachment. Such effects can determine a loss of draft height in the channel-chimney system.

References

Agarwal, R. and Jaluria, Y. (1989), "Deflection of a two-dimensional natural convection wake due to the presence of a vertical surface in close proximity", *Journal of Fluid Mechanics*, Vol. 201, pp. 35-56.

Andreozzi, A., Buonomo, B. and Manca, O. (2005), "Numerical study of natural convection in vertical channels with adiabatic extensions downstream", *Numerical Heat Transfer, Part A*, Vol. 47, pp. 741-62.

Andreozzi, A., Buonomo, B. and Manca, O. (2009), "Thermal management of a symmetrical heated channel-chimney system", *International Journal of Thermal Sciences*, Vol. 48, pp. 475-87.

Asako, Y., Nakamura, H. and Faghri, M. (1990), "Natural convection in a vertical heated tube attached to a thermally insulated chimney of a different diameter", *ASME Journal of Heat Transfer*, Vol. 112, pp. 790-5.

Auletta, A. and Manca, O. (2002), "Heat and fluid flow resulting from the chimney effect in a symmetrically heated vertical channel with adiabatic extensions", *International Journal of Thermal Sciences*, Vol. 41, pp. 1101-11.

Auletta, A., Manca, O., Morrone, B. and Naso, V. (2001), "Heat transfer enhancement by the chimney effect in a vertical Isoflux channel", *International Journal of Heat and Mass Transfer*, Vol. 44, pp. 4345-57.

Ayinde, T.F., Said, S.A.M. and Habib, M.A. (2006), "Experimental investigation of turbulent natural convection flow in a channel", *Heat and Mass Transfer*, Vol. 42, pp. 169-77.

Bacharoudis, E., Vrachopoulos, M.G., Koukou, M.K., Margaris, D., Filios, A.E. and Mavrommatis, S.A. (2007), "Study of the natural convection phenomena inside a wall solar chimney with one wall adiabatic and one wall under a heat flux", *Applied Thermal Engineering*, Vol. 27, pp. 2266-75.

Bejan, A. (2000), *Shape and Structure from Engineering to Nature*, Cambridge University Press, New York, NY.

Campo, A., Manca, O. and Morrone, B. (1999), "Numerical analysis of partially heated vertical parallel plates in natural convective cooling", *Numerical Heat Transfer, Part A*, Vol. 36, pp. 129-51.

Fisher, T.S. and Torrance, K.E. (1999), "Experiments on chimney-enhanced free convection", *ASME Journal of Heat Transfer*, Vol. 121, pp. 607-8.

Gebhart, B., Jaluria, Y., Mahajan, R. and Sammakia, B. (1988), *Buoyancy-induced Flows and Transport*, Hemisphere, Washington, DC.

Haaland, S.E. and Sparrow, E.M. (1983), "Solutions for the channel plume and the parallel-walled chimney", *Numerical Heat Transfer*, Vol. 6, pp. 155-72.

Harris, D.J. and Helwig, N. (2007), "Solar chimney and building ventilation", *Applied Energy*, Vol. 84, pp. 135-46.

Jorg, O. and Scorer, R.S. (1967), "An experimental study of cold inflow into chimneys", *Atmospheric Environment*, Vol. 1, pp. 645-54.

Kazansky, S., Dubovsky, V., Ziskind, G. and Letan, R. (2003), "Chimney-enhanced natural convection from a vertical plate: experiments and numerical simulations", *International Journal of Heat and Mass Transfer*, Vol. 46, pp. 497-512.

Kim, S.J. and Lee, S.W. (1996), *Air Cooling Technology for Electronic Equipment*, CRC Press, Boca Raton, FL.

Ledezma, G.A. and Bejan, A. (1997), "Optimal geometric arrangement of staggered vertical plates in natural convection", *ASME Journal of Heat Transfer*, Vol. 119, pp. 700-8.

Lee, K.T. (1994), "Natural convection in vertical parallel plates with an unheated entry or unheated exit", *Numerical Heat Transfer, Part A*, Vol. 25, pp. 477-93.

Letan, R., Dubovsky, V. and Ziskind, G. (2003), "Passive ventilation and heating by natural convection in a multi-story building", *Building and Environment*, Vol. 38, pp. 197-208.

Manca, O., Musto, M. and Naso, V. (2001), "Experimental analysis of chimney effect in a vertical Isoflux channel", *Proceedings of the 5th World Conference on Experimental Heat Transfer, Fluid Mechanics and Thermodynamics, ExHFT5, Thessaloniki, Greece*, Vol. 1, pp. 645-50.

Manca, O., Musto, M. and Naso, V. (2002), "Flow visualization and air temperature measurements in symmetrically heated vertical channels with adiabatic extensions", *Proceedings of IMECE-ASME, IMECE2002-32985, New Orleans, LA*.

Manca, O., Morrone, B., Nardini, S. and Naso, V. (2000), "Natural convection in open channels", in B. Sunden and G. Comini (Eds.), *Computational Analysis of Convection Heat Transfer*, WIT Press, Southampton, pp. 235-78.

Modi, V. and Moore, F.K. (1987), "Laminar separation in buoyant channel flows", *Journal of Fluid Mechanics*, Vol. 177, pp. 37-47.

Modi, V. and Torrance, K.E. (1987), "Experimental and numerical studies of cold inflow at the exit of buoyant channel flows", *ASME Journal of Heat Transfer*, Vol. 109, pp. 392-404.

Moore, F. (1978), "Cold inflow and its applications for dry tower design", *Proceedings of 2nd Conference on Waste Heat Management and Utilization, University of Miami, Miami Beach, FL*.

Oosthuizen, P.H. (1984), "A numerical study of laminar free convective flow through a vertical open partially heated plane duct", *ASME HTD – Fundamentals of Natural Convection-Electronic Equipment Cooling*, Vol. 32, pp. 41-8.

Pelletier, D. and Roache, P.J. (2006), "Verification and validation of computational heat transfer", in Minkowicz, W.J., Sparrow, E.M. and Murthy, J.Y. (Eds), *Handbook of Numerical Heat Transfer*, John Wiley and Sons, Hoboken, NJ, pp. 417-42.

Roache, J.P. (1998), *Computational Fluid Dynamics*, Hermosa, Albuquerque, NM.

Sparrow, E.M., Chrysler, G.M. and Azevedo, L.F.A. (1984), "Observed flow reversal and measured-predicted nusselt numbers for natural convection in one-sided heated vertical channel", *ASME Journal of Heat Transfer*, Vol. 106, pp. 325-37.

Straatman, A.G., Tarasuk, J.D. and Floryan, J.M. (1993), "Heat transfer enhancement from a vertical, isothermal channel generated by the chimney effect", *ASME Journal of Heat Transfer*, Vol. 115, pp. 395-402.

Thrasher, W.W., Fisher, T.S. and Torrance, K.E. (2000), "Experiments on chimney-enhanced free convection from pin-fin heat sink", *Journal of Electronic Packaging*, Vol. 122, pp. 350-5.

Torrance, K.E. (1985), *Handbook of Heat Transfer - Fundamentals*, chapter 5, 2nd ed., McGraw-Hill, New York, NY.

Yilmaz, T. and Fraser, S.M. (2007), "Turbulent natural convection in a vertical parallel-plate channel with asymmetric heating", *International Journal of Heat and Mass Transfer*, Vol. 50, pp. 2612-23.

Yilmaz, T. and Gilchrist, A. (2007), "Temperature and velocity field characteristics of turbulent natural convection in a vertical parallel-plate channel with asymmetric heating", *Heat and Mass Transfer*, Vol. 423, pp. 707-19.

Corresponding author
Assunta Andreozzi can be contacted at: assunta.andreozzi@unina.it